

Utilization of a Novel Chitosan/Clay/Biochar Nanobiocomposite for Immobilization of Heavy Metals in Acid Soil Environment

Hoda Arabyarmohammadi¹ · Ahmad Khodadadi Darban¹ · Mahmoud Abdollahy¹ · Raymond Yong² · Bitā Ayati³ · Abbas Zirakjou⁴ · Sjoerd E. A. T. M. van der Zee^{5,6}

Published online: 15 September 2017

© The Author(s) 2017. This article is an open access publication

Abstract An organic–inorganic composite of chitosan, nanoclay, and biochar (named as MTCB) was chosen to develop a bionanocomposite to simultaneously immobilize Cu, Pb, and Zn metal ions within the contaminated soil and water environments. The composite material was structurally and chemically characterized with the XRD, TEM, SEM, BET, and FT-IR techniques. XRD and TEM results revealed that a mixed exfoliated/intercalated morphology was formed upon addition of small amounts of nanoclay (5% by weight). Batch adsorption experiments showed that the adsorption capacity of MTCB for Cu²⁺, Pb²⁺, and Zn²⁺ were much higher than that of the pristine biochar sample (121.5, 336, and 134.6 mg g⁻¹ for Cu²⁺, Pb²⁺, and Zn²⁺, respectively). The adsorption isotherm for Cu²⁺ and Zn²⁺ fitted satisfactorily to a Freundlich model while the isotherm of Pb²⁺ was best represented by a Temkin model. That the adsorption capacity increased with increasing temperature is indicative of the endothermic nature of the adsorption process. According to the FTIR analysis, the main mechanism involved in

immobilization of metals is binding with –NH₂ groups. Results from this study indicated that modification of biochar by chitosan/clay nanocomposite enhances its potential capacity for immobilization of heavy metals, rendering the bionanocomposite into an efficient heavy metal sorbent in mine-impacted acidic waters and soils.

Keywords Heavy metals · Nanobiocomposite · Biochar · Soil · Immobilization · SPLP

Introduction

Mineral and metallurgical processes are major sources of soil pollution worldwide. These industrial activities use large volumes of water and produce huge amounts of different types of wastes. Mine tailings, for instance, form an important source of heavy metals with high concentrations of Cu, Pb, Zn, Cd, Cr and As [1]. Often, these tailings are rich in sulfide minerals which are readily oxidized when exposed to water and air to produce sulfuric acid. Under such (very) acid conditions, heavy metals become mobile and are easily leached out of the tailing deposits. Therefore, both tailings and their leaching water are known to lead to soil contamination [2] and necessitate measures to mitigate or prevent heavy metals contamination. For this purpose, various physicochemical mechanisms are known to render metals immobile and biologically unavailable [3]. There are several techniques have been developed for remediating mine tailings such as landfilling, thermal treatment, electro reclamation and soil capping. However, all are costly and environmentally unfavorable since at the end, they end in toxic solid/liquid residues which will require an engineered safe disposal, as well [4].

✉ Ahmad Khodadadi Darban
akdarban@modares.ac.ir

¹ Mineral Processing Group, Mining Engineering Department, Tarbiat Modares University, Tehran, Iran

² William Scott Professor Emeritus of Civil Engineering, McGill University, Montreal, QC, Canada

³ Civil and Environmental Engineering Department, Tarbiat Modares University, Tehran, Iran

⁴ Nanomaterials Group, Materials Engineering Department, Tarbiat Modares University, Tehran, Iran

⁵ Soil Physics and Land Management Group, Wageningen University, Wageningen, The Netherlands

⁶ School of Chemistry, Monash University, Melbourne, VIC, Australia

It has been shown that biochars are efficient soil amendments to improve soil quality and they are now being commercialized in many countries. The main interesting property of this carbonic material is its high stability and resistance against degradation in soil systems [5]. Because of this feature, biochar maintains the nutrient and water retention capacities in soil, which is of agricultural importance. Additionally, contaminants as toxins, and organic pollutants such as PAHs are immobilized for large time periods [5]. Also regarding the immobilization of heavy metals in soil, use of biochar has been a prominent subject of research [1, 6].

Acid copper mine tailings are commonly found in the Sarcheshmeh Copper Complex, where soil is contaminated with several metals such as Cu, Zn, and Pb. Although biochars have been proposed as a candidate sorbent for these metals, the sorption capacities of most biochars for many heavy metals are smaller than that of some commercial adsorbents [7]. Accordingly, the aim of the present research was to enhance the sorption capacity of biochar through designing a novel biochar-based composite.

Chitosan, one of the most widely used and naturally abundant biopolymers, contains acetamido and amino groups [8]. The presence of these functional groups gives chitosan a cationic polyelectrolyte character and enables it to chelate metal ions [9, 10]. Since it is a hydrophilic biopolymer, it is potentially biocompatible, environmentally friendly, and suitable to be used in sustainable materials (e.g. adsorbents, coating materials, membranes) [8, 9]. Nanoclays including modified and unmodified montmorillonite clays (commercially referred to as the Cloisite series) are widely used as nanofillers or additive materials to improve various physical properties of polymers, such as reinforcement. Montmorillonite clay (MT) is a phyllosilicate formed of Al–O octahedral platelets sandwiched between two Si–O tetrahedral sheets. The remarkably large adsorption capacity of this material for metals is mainly due to the specific layered structure and existence of exchangeable hydrated cations [11]. Chitosan based nanocomposites containing MT have been used for dye removal [9, 12–15] and sorption of heavy metals [16–19] from effluents. However, their effect on contaminated soils has not yet been evaluated. Therefore, a second aim of this investigation is to assess the performance of this nanocomposite structure within the soil environment, it is employed onto a sustainable charred matrix material to form a bionanocomposite. The behavior of chitosan/clay modified biochar in immobilization of heavy metals has been investigated afterwards.

Materials and Methods

Chemicals

All chemical reagents were of the highest purity that is commercially available. Lead (II) nitrate, copper (II) nitrate, zinc (II) nitrate, sodium chloride, potassium nitrate, acetic acid, nitric acid, sulfuric acid, and sodium hydroxide were purchased from Merck (Merck Millipore, Germany). Chitosan was from Sigma-Aldrich. The source clay, sodium MT (Cloisite Na⁺), was purchased from Southern Clay Products, Gonzales, TX. The cation exchange capacity (CEC) of Cloisite Na⁺ is $92.6 \times 10^{-5} \text{ mol}_c \text{ g}^{-1}$ as reported by suppliers (mol_c stands for mol-charge, formerly called equivalent). Distilled, deionized water (DDW) was used for all procedures.

Soil Sample

The simulated soil was prepared by mixing 50% sand, 35% silt, and 15% kaolinite according to the mean texture of the polluted soils in vicinity of Sarcheshmeh Copper Mine Complex, Kerman, Iran. The contaminated area is about 400 km² of the area and mainly involves the top 15 centimeters of soil. The main contamination concerns the metals Cu, Pb, and Zn. The soil is classified as silty sand (SM) according to ASTM D422 and the Unified Soil Classification System (USCS).

Preparation of Chitosan/Clay/Biochar Nanobiocomposites

Residual bark chips were collected from Mazandaran Wood and Paper plant site to be used as feedstock and were air-dried overnight. The bark sample was pyrolysed at 600 °C at 10 °C min⁻¹ and 2 h residence time under 3 L min⁻¹ nitrogen flow in a chamber furnace (Nabertherm, Germany). The pyrolysis conditions were chosen according to the thermal analysis over the biomass which was performed in advance. The resulting chars were allowed to cool to room temperature, rinsed several times with DDW, dried at 80 °C in oven, and sieved to <2 mm. A chitosan aqueous solution was prepared by dissolving 5 g of chitosan powder in 250 ml acetic acid solution (2% v/v). A nanoclay suspension with 5% clay content was prepared by dispersing appropriate amounts of clay in 10 ml of 2% acetic acid and stirring for 24 h. Afterwards, the chitosan solution was gradually added to the pretreated clay suspension. The final mixture was vigorously stirred for another 24 h at 60 °C. Finally, 5 g of biochar was added to the mixture and stirred for 30 min to provide a homogeneous suspension. The biochar/chitosan/clay suspension was then added drop wise into a 1000 ml NaOH (1.2%) solution and

kept in the solution for 12 h. Afterwards, the composite material (MTCB) was filtered, washed several times with DDW, and oven dried at 70 °C.

Characterization

Prior to pyrolysis, to find the proper temperature for charring the biomass, a thermogravimetric analysis (TGA) was performed under nitrogen flow from room temperature to 700 °C at a rate of 10 °C min⁻¹ over the bark sample using a Mettler Toledo TGA1 device. The biomass was then pyrolyzed and the obtained biochar from this stage was used as a base matrix for developing the composite material. Total C, H, N, S, and O content in the base char was determined by a CHN Elemental analyzer (Costech ECS 4010). Moreover, the total P content was measured by the acid digestion procedure according to Kuo [20]. The basal spacing of the clay was determined with a Philips X'Pert MPD X-ray diffractometer with a Co-K α radiation source and scans were carried out for diffraction angles below 10°. The dispersion of chitosan among the clay platelets was also monitored optically using a transmission electron microscope (Zeiss EM 900) under an accelerating voltage of 80 kV. Ultra-Thin films (<100 nm) for this purpose were prepared by cutting from the epoxy block with the embedded nanocomposite sample at room temperature using a Leica Reichert OMU3 ultramicrotome. The Brunauer, Emmett, and Teller (BET) specific surface area and porosity were determined using a Belsorp mini II device. Surface morphology and elemental composition and distribution were observed over gold-coated samples using a Tescan MIRA3 LM FE-SEM equipped with a SAMx SDD energy dispersive detector. The FT-IR spectroscopy of the samples was conducted at room temperature with KBr pellets on a Bruker vertex70 FT-IR device.

The point of zero charge (pH_{PZC}) of the MTCB was determined using the solid addition method [20, 21]. 20 ml of 0.01 M KNO₃ was transferred to a series of 50 ml flasks. The initial pH values (pH₀) of the series were adjusted in a 2–12 range by adding either 0.01 N HNO₃ or NaOH. The final total volume of the solution in each flask was then exactly set to 25 ml by adding the proper amount of KNO₃ solution of the same ionic strength. After the pH₀ of the solutions were accurately recorded, 0.1 g of MTCB was added to each flask which was immediately recapped. The suspensions were then intermittently shaken for 48 h to reach the equilibrium. Finally, the pH_{ZPC} was determined by plotting δ pH (the difference between the initial pH₀ and final pH_f) against the pH₀, and designating the point of intersection in the resulting curve. The procedure was repeated for 0.1 M KNO₃.

Metal Adsorption Experiments in Aqueous Solution

Single-Element Batch Adsorption Experiments

Individual stock solutions for Cu²⁺, Pb²⁺, and Zn²⁺ were prepared by dissolving proper amounts of their nitrate salts into 0.01 M NaCl as background electrolyte. Adsorption tests were conducted by agitating 0.25 g of MTCB sample in 25 ml of single-element metal-containing solutions at 0.5, 1, 2, 3, 4, 5, 10, 20, 30, 40, 50, and 51 mM concentrations, for 24 h at different temperatures of 25, 40, and 60 °C until equilibrium was established. The pH of the system was adjusted at 5 by adding proper amount of diluted HNO₃. At the end of each test, the suspension was filtered and the filtrate was acidified to pH <2 for AAS analysis (Varian AA240, Australia). The residue was rinsed with DDW, dried and stored. Each test was duplicated and averaged. The amount of each metal uptake at equilibrium q_e (mg g⁻¹) was calculated by:

$$q_e = (C_0 - C_e)V/W$$

where C_0 and C_e (mg L⁻¹) are initial (t=0) and equilibrium metal concentrations, respectively, V is the volume of the solution (L) and W is the used mass of dry MTCB (g).

A similar procedure was performed for batch kinetic experiments, repeating a 24 h adsorption test in case of 4 mM concentration of each metal. Samples were withdrawn by removing 10 mL aliquots out of the initial 500 ml solution at predetermined time intervals within the 24 h. The amount of adsorbed metal at time t , q_t (mg g⁻¹), was calculated by:

$$q_t = (C_0 - C_t)V/W$$

where C_t (mg L⁻¹) is metal concentration at time t .

To evaluate and compare the adsorption capacities of Cu²⁺, Zn²⁺, and Pb²⁺ onto MTCB, the most common adsorption isotherm models namely Langmuir, Freundlich, Temkin, and Dubinin–Radushkevich (D–R) were used to analyze the experimental data (Table 1). In the Langmuir isotherm model is assumed that adsorption occurs on homogeneous surface in monolayer coverage and no interaction between

Table 1 Isotherm functions and their parameters [23]

Isotherm	Isotherm function	Parameters
Langmuir	$q_e = \frac{Q_{max}K_L C_e}{1+K_L C_e}$	Q_{max} (mg g ⁻¹) K_L (L mg ⁻¹)
Freundlich	$q_e = K_F C_e^{1/n}$	K_F (L mg ⁻¹) ^{1/n} n
Temkin	$q_e = \frac{RT}{b_T} \ln(K_T C_e)$ $Q_{max} = \frac{RT}{b_T}$	Q_{max} (mg g ⁻¹) K_T (L g ⁻¹)
D–R	$q_e = Q_{max} \exp(-D\epsilon^2)$ $\epsilon = RT \ln\left(1 + \frac{1}{C_e}\right)$	Q_{max} (mg g ⁻¹) D (mol ² kJ ⁻²)

sorbed molecules. Also, a uniform energy of adsorption onto the surface and no transmigration of adsorbate in the surface plane are among the Langmuir model's assumptions. In the Freundlich model, multilayer adsorption on the heterogeneous solid surface of the adsorbent is assumed, where stronger binding sites are occupied first and the binding strength declines with increasing adsorbed quantity [22]. In the Temkin model, the decline of the heat of adsorption is not logarithmic [23] but linear as the adsorption proceeds towards the saturation point and the distribution of binding energy at all sites is uniform. In other words, it considers the effects of some indirect adsorbate/adsorbate interactions on the isotherm and suggests a linear decrease for heat of adsorption of all the molecules in the layer with coverage consequently [24]. The Dubinin–Radushkevich model is especially suitable for describing the adsorption onto porous materials.

In Table 1, q_e is the amount of the metal uptake per unit mass of MTCB (mg g^{-1}), C_e is the equilibrium concentration of metal (mg L^{-1}), Q_{max} is the maximum loading capacity, K_L is a constant related to the affinity, K_F and n are indicators of adsorption capacity and intensity in Freundlich isotherm, respectively. In the Temkin model, K_T is the isotherm constant and b_T is a constant related to heat of adsorption. Finally, in the D–R model, D is the constant of the adsorption energy ($\text{mol}^2 \text{kJ}^{-2}$), which is related to the average energy of adsorption per unit mole of the adsorbate, energy needed for the transfer from infinite distance to the surface of the adsorbent, and ε is the Polanyi potential. T is absolute solution temperature (K) and R is the universal gas constant (equal to $8.314 \text{ J mol}^{-1} \text{ K}^{-1}$).

Application of D–R isotherm helps determine the chemical or physical nature of the adsorption process. The value of mean adsorption energy, E (kJ mol^{-1}), can be obtained from D–R parameter D using the following equation

$$E = \frac{1}{\sqrt{2D}}$$

The value of E ranges from 1 to 8 kJ mol^{-1} in case of physical adsorption to $8\text{--}16 \text{ kJ mol}^{-1}$ for chemical adsorption [25].

Isotherm parameters are determined through non-linear regression, setting the average relative error (ARE) to zero if using the Solver add-in function of Microsoft Excel. The ARE has been calculated between experimental and calculated values and is given in

$$ARE = \frac{100}{n} \sum_{i=1}^n \left| \frac{q_{e \text{ calc}} - q_{e \text{ exp}}}{q_{e \text{ exp}}} \right|_i$$

where $q_{e \text{ calc}}$ and $q_{e \text{ exp}}$ are calculated and experimental equilibrium capacity, respectively, and n is the number of

experiments. Obviously, lower ARE represents the best fit model.

The rate-controlling steps during the adsorption of each metal were further identified by kinetic studies. In this regard, second order, pseudo-second order, Elovich and intra-particle diffusion kinetic models were applied (Table 2). The best-fit kinetic model was obtained by non-linear regression method with the lowest ARE value.

Multi-Element Batch Adsorption Experiment

A suspension of 10 g L^{-1} MTCB in background electrolyte (0.01 M NaCl) was prepared and equilibrated for 24 h. After pH measurement (Metrohm 827 pH lab, Switzerland), Cu^{2+} , Zn^{2+} , and Pb^{2+} (as their nitrate salts) were added simultaneously, so that the final concentration of each metal in the reactor reached 4 mM . The reactor was agitated for another 24 h and after pH measurement, the suspension was filtered and the filtrate was acidified to $\text{pH} < 2$ for AAS analysis. The experiment was duplicated and averaged. All the tests were performed at room temperature.

Immobilization of Cu^{2+} , Pb^{2+} , and Zn^{2+} in Soil

Synthetic rain water (SRW) was prepared by adding a diluted sulfuric/nitric acid mixture (60/40 w/w) to DDW until $\text{pH} 4.2$ according to EPA method 1312. The synthetic precipitation leaching procedure (SPLP) was performed as 10 g of the soil sample amended with 10% MTCB ($w_{\text{char}}/w_{\text{soil}}$) was equilibrated in SRW (20 g L^{-1}) for 24 h in an end-over-end shaker. After pH measurement, Cu^{2+} , Zn^{2+} , and Pb^{2+} (again as their nitrate salts) were added simultaneously for the final concentration of 4 mM for each metal. The reactor was agitated for another 24 h, the pH was measured, the suspension was centrifuged, the supernatant was filtered, and the filtrate was acidified to $\text{pH} < 2$ for AAS analysis.

Table 2 Kinetic models and their parameters

Kinetic model	Equation	Parameters	Ref.
Second order	$q_t = q_e / (1 + q_e k_2 t)$	q_e (mg g^{-1}) k_2 ($\text{g mg}^{-1} \text{ h}^{-1}$)	[23]
Pseudo-second order	$q_t = k_{2p} q_e^2 t / (1 + q_e k_{2p} t)$	q_e (mg g^{-1}) k_{2p} (h^{-1})	
Elovich	$q_t = \frac{1}{\beta} \ln(\alpha \beta t)$	β (mg^{-1}) α ($\text{mg g}^{-1} \text{ h}^{-1}$)	
Intra-particle diffusion	$q_t = k_{id} t^{1/2} + I$	k_{id} ($\text{mg g}^{-1} \text{ h}^{-0.5}$)	[38]

Results and Discussion

Determination of the Proper Pyrolysis Conditions

The biomass was initially subjected to the thermal analysis. Result of TGA over the bark chips is shown in Fig. 1. According to the results, the initial mass loss was approximately 10% and mainly due to moisture evaporation. Devolatilization and biomass thermal decomposition were responsible for most of the loss of mass (approximately 70%). The same mass loss steps may be deduced based on the obvious peak values in DTA curve. It should be noted that the characteristic thermal decomposition of hemicellulose, cellulose and lignin, as the main constituent of the biomass, are reported to be at 200–350, 320–400, and 250–550 °C, respectively [26]. Accordingly, the pyrolysis conditions were selected as 600 °C at 10 °C min⁻¹ and 2 h residence time, which made the char more recalcitrant, by degrading the main biopolymers and increasing the number of aromatic compounds.

Characterization of the Base Biochar

The obtained char was analyzed for its C, H, N, S, O, and P content (Table 3). The O/C and H/C ratios are <0.2 and <0.4, respectively, which indicates that the obtained biochar has high carbon sequestration potential [27].

FE-SEM micrographs reveal the nanoporous texture for the biochar (Fig. 2a). This was also confirmed by the value of the mean pore diameter obtained by BET analysis

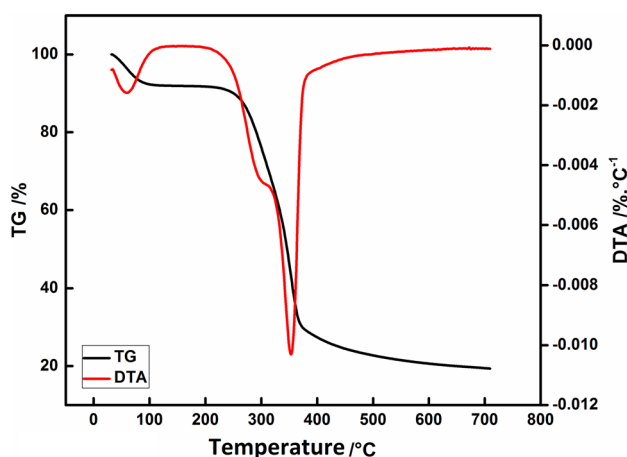


Fig. 1 Thermogravimetric and derivative thermogravimetric mass loss curves

Table 3 Elemental composition of the pristine biochar

Element	C	H	N	S	O	P
Mass percent	77.74	1.92	0.66	0.55	11.15	0.134

(Table 4), since the high value of the total surface area also indicates a highly porous matrix for the pristine biochar. The nitrogen adsorption–desorption isotherm (Fig. 2b) shows a dramatic rise in N₂ adsorption at relative pressures less than 0.1, which is due to the presence of micropores (pores with diameters up to 2 nm) [28]. At higher relative pressures, the adsorption of the gas into mesopores (pores with diameters within 2–50 nm) of biochar occurs where along with the formation of multimolecular layers, condensation of the gaseous molecules takes place in what is called capillary condensation [28]. The shape of adsorption isotherms can provide qualitative information on the adsorption process and the extent of the surface area available to the adsorbate. The experimental isotherm follows a combination of type I and IV with a mixed micro/mesoporous structure, according to the IUPAC classification [29]. Various data could be calculated using different analysis methods such as BJH and t-plot (Table 4). These data confirm that the microporosity in the biochar is high enough to be used as a base matrix in the nanocomposite adsorbent. The BJH pore distribution is also given in Fig. 2b.

Characterization of the Final Hybrid

A chitosan/clay/biochar nanobiohybrid (MTCB) was designed and developed and resulted in a composite with the simultaneous advantage of the chelating behavior of chitosan, the lamellar adsorptive properties of clay (MT), and the nanoporosity of the base biochar.

XRD is a useful method for investigating the mode of MT and chitosan engagement (e.g. tactoids, intercalation, or exfoliation) [8]. Figure 3a illustrates a comparison between X-ray diffraction patterns of MT and MTCB. The XRD pattern of MT shows a reflection at $2\theta = 8.88^\circ$ for the basal 001 lattice spacing of silicate layer, whereas there is no characteristic reflection in the pattern related to MTCB. This possibly confirms the formation of a partial exfoliated MT dispersion in the chitosan matrix [30]. In fact, the poly-cationic nature of chitosan enables its easy adsorption onto the negatively charged layers of MT. In this process, the intrusion of chitosan into clay interlayer spaces forces the platelets apart, increasing the d-value. This process may continue until the platelets are completely separated and distributed within the chitosan matrix [31]. However, definitive conclusions on the basis of XRD alone about the structure may not suffice [8] and TEM techniques are

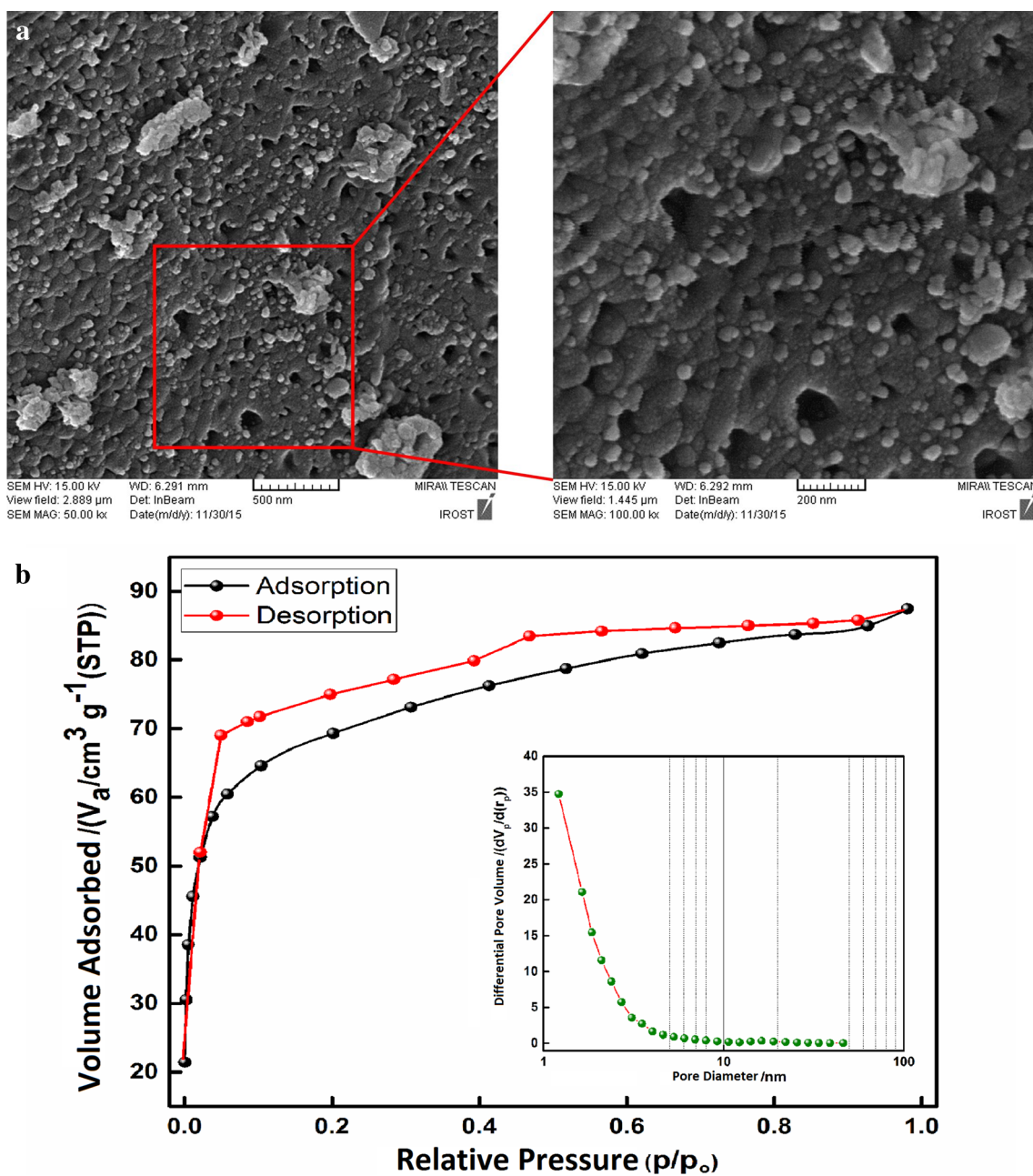


Fig. 2 FE-SEM micrographs (a), and adsorption–desorption diagram and BJH pore volume distribution (b) (adsorbate: N₂, adsorption temperature: 77 K) of the pristine biochar sample

Table 4 Parameter values obtained from the nitrogen adsorption isotherm

Total surface area/ (m ² g ⁻¹)	Mean pore diameter / nm	Total pore volume/ (cm ³ g ⁻¹)	Micropore volume ^a / (cm ³ g ⁻¹)	Mesopore volume ^b / (cm ³ g ⁻¹)
272.49	1.9842	0.1352	0.1262	5.0116 × 10 ⁻²

^aCalculated from t-plot

^bCalculated from BJH

also necessary for characterizing the morphology of the MTCB. TEM images show the perfect dispersion of MT in the chitosan matrix so that mixed intercalated and exfoliated structures were obtained (Fig. 3b).

FE-SEM micrographs also show three different phases indicating the heterogeneous structure of the MTCB (Fig. 4a, b) comprising the flaky amorphous nature of chitosan [17], the porous structure of the biochar, and the curly and delaminated sheets of nanoclay [32] with much smaller sizes scattered within the chitosan. The amount of

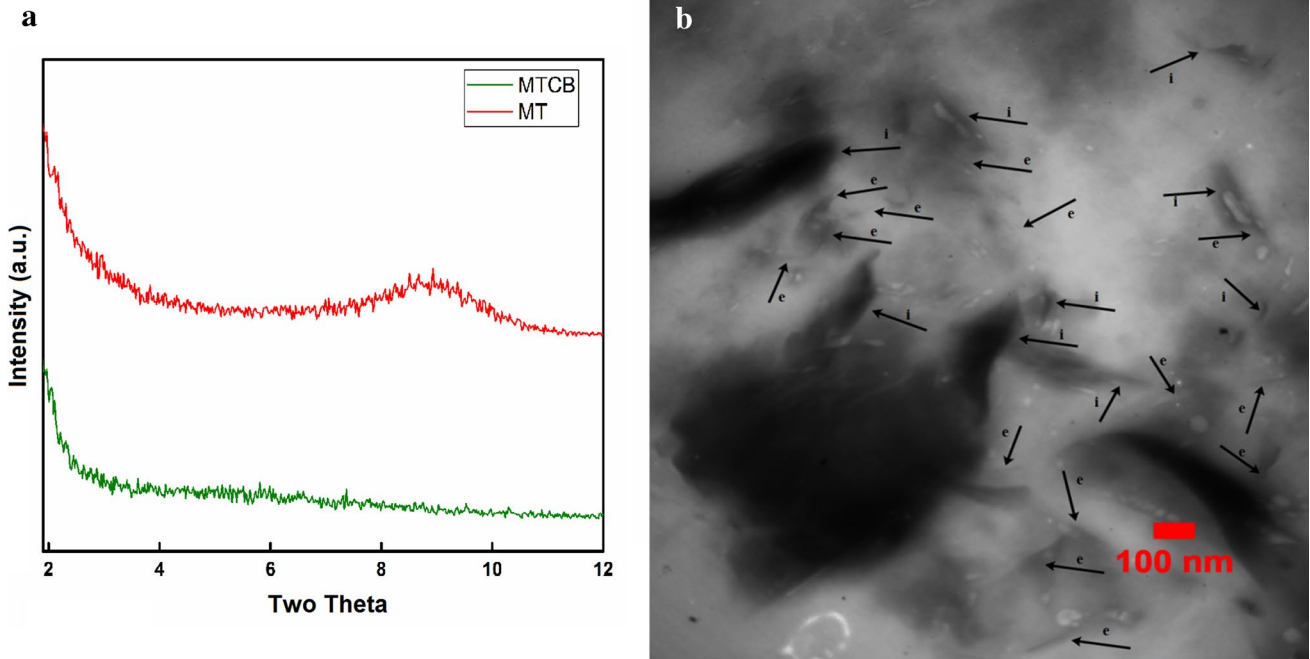
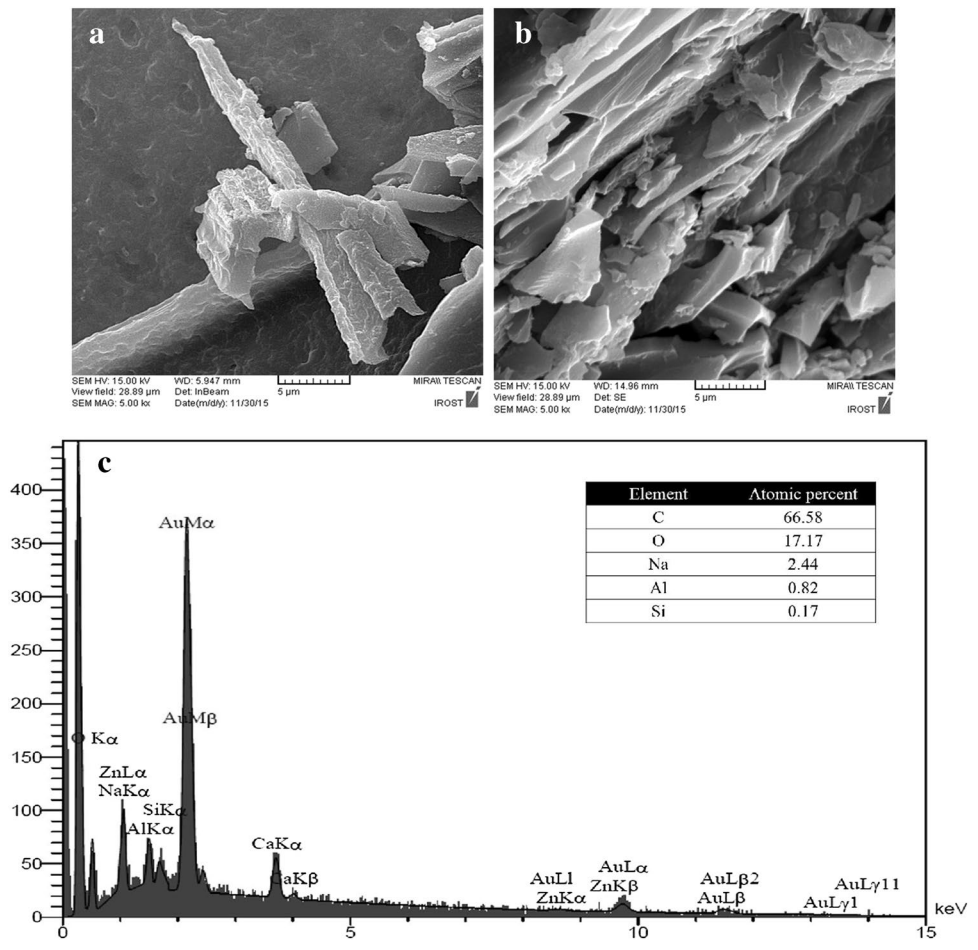


Fig. 3 **a** Comparison of XRD patterns related to the original Cloisite- Na^+ (MT) and the clay/chitosan/biochar nanobiocomposite (MTCB), and **b** TEM micrograph showing the intercalated (i) and exfoliated (e) silicate layers appearing as sharp lines on a grey background from the matrix

Fig. 4 FE-SEM micrographs (**a** and **b**) and EDS analysis (**c**) of MTCB (outstanding peak of Au is related to the sputtered gold layer during preparation step)



Si, Al, and Na may represent the dispersed Na-clay particles within the matrix (Fig. 4c). The strong interaction between the matrix and silicate layers in MTCB are due to the hydrogen bonds formed between amino and hydroxyl functional groups in each chitosan unit and the silicate hydroxylated edge groups [8].

Active functional groups present on the MTCB surface are evaluated by studying the FT-IR spectrum. Figure 5 shows the spectra of pure chitosan (PC) and MTCB for comparison. In the FT-IR spectrum of PC, the bands near 3300 cm^{-1} are attributed to stretching vibrations of the O–H and N–H groups, whereas those near 2900 cm^{-1} correspond to aliphatic C–H stretching vibrations. Additionally, the band at 1648 cm^{-1} corresponds to the protonated amine group in chitosan, while the one at 1561 cm^{-1} corresponds to the $-\text{NH}_2$ band. The bands near 1400 cm^{-1} can be attributed to deformation vibrations of aliphatic C–H groups. The spectrum of MTCB sample shows the combination of characteristic bands due to chitosan and clay. The shifting of the N–H deformation band from 1561 cm^{-1} in pure chitosan to 1660 cm^{-1} in MTCB indicated the interaction of the negatively charged MT surfaces with the protonated amine groups ($-\text{NH}_3^+$) of chitosan. The bands corresponding to the C–H deformation modes of chitosan were also shifted as a result of the chitosan-clay layers interactions.

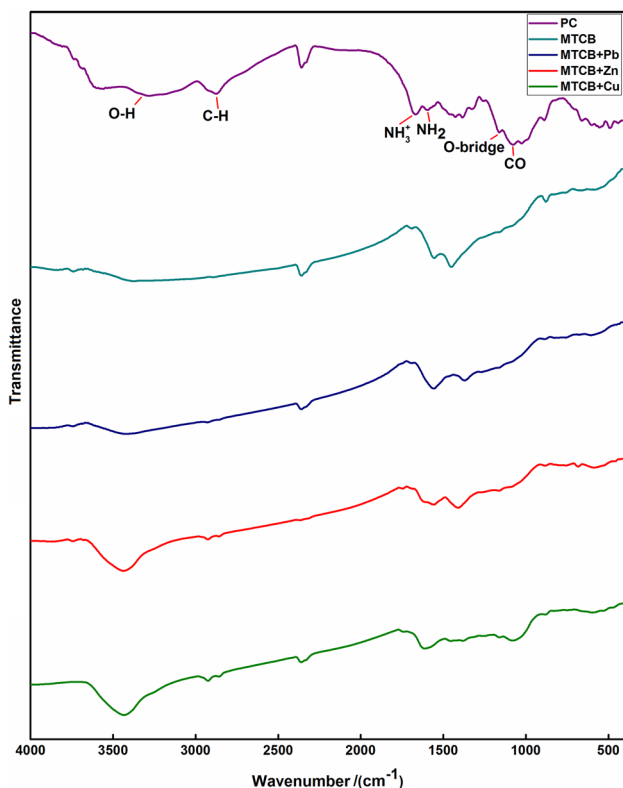


Fig. 5 FT-IR spectra of PC and MTCB (pre and post sorption samples)

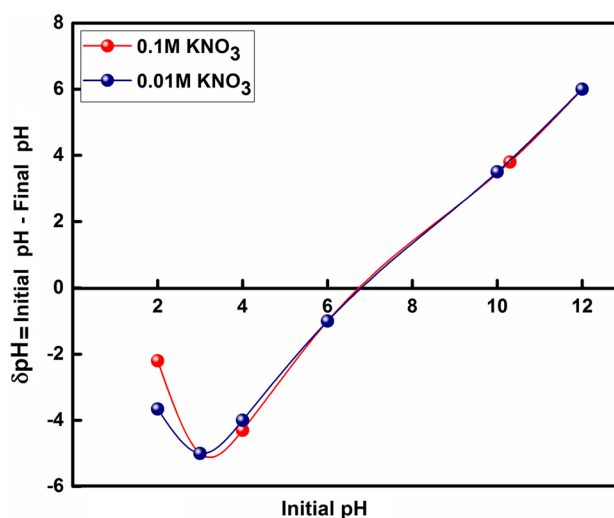


Fig. 6 Point of zero charge (pH_{PZC}) of MTCB

The point of zero charge was determined by the solid addition method. Figure 6 represents the plot of ΔpH versus initial pH value for the MTCB at two different KNO_3 concentrations of 0.01 and 0.1 M. The intersection point of both curves with the horizontal axis obviously coincide at pH 6.8. This indicates that pH_{PZC} for MTCB is at pH 6.8.

Single-Element Batch Adsorption Experiments

Figure 7 shows the results of single-element batch adsorption tests done for the 12 different initial concentrations. The loading capacity increased as higher initial concentration was used in experiments and finally leveled off at 50 mM concentration. This implies that the maximum sorption capacity of the nanocomposite at $25\text{ }^\circ\text{C}$ for copper, lead and zinc is 121.5 , 336 , and 134.6 mg g^{-1} , respectively. According to Fig. 7, a higher temperature favored metal ions adsorption onto MTCB suggesting that the adsorption onto MTCB was an endothermic process enabling the metal ions to overcome the diffuse double layer and adsorb onto the composite's interior structure provided the sufficient energy at elevated temperatures. Earlier research [31, 32] suggested the same. Table 5 lists the details of isotherms fitting data. According to the *ARE* values, sorption of copper and zinc onto MTCB is in agreement with the Freundlich, isotherm while lead sorption isotherm is better described by the Temkin model.

The kinetic data obtained from single-element batch reactor tests are also shown in Fig. 8a. Non-linear regression of the kinetics of copper, zinc, and lead sorption onto MTCB composite are best described by the pseudo-second order model (Table 6). Such a kinetic model agrees well with the occurrence of both chemical reaction and physical diffusion process [33, 34].

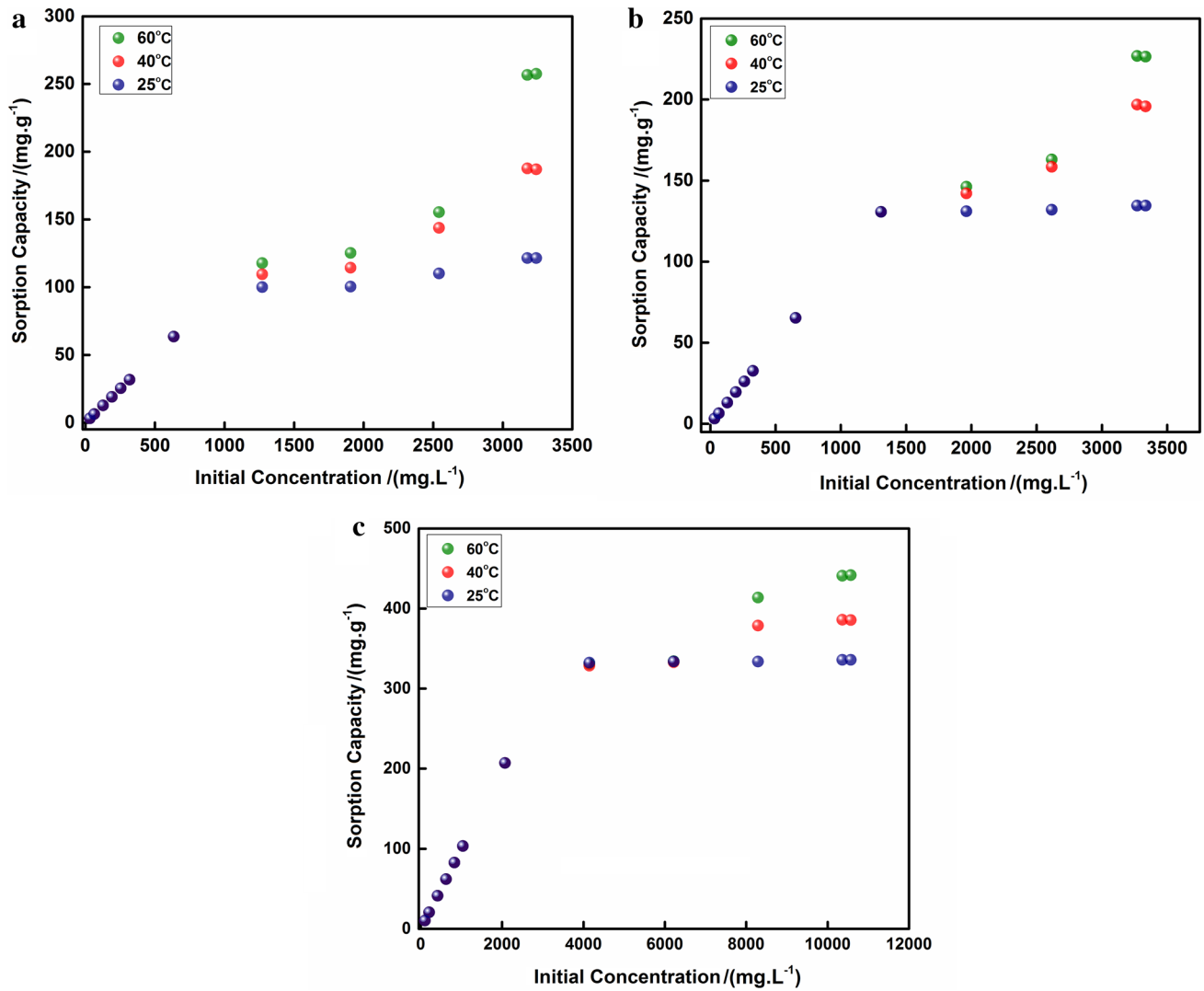


Fig. 7 Individual variations of **a** copper, **b** zinc, and **c** lead sorption capacity against initial metal concentration for different temperatures (25, 40, and 60 °C)

Table 5 Constants and ARE of langmuir, freundlich, temkin and D–R models for Cu²⁺, Zn²⁺, and Pb²⁺ adsorption onto MTCB (adsorbent dose 10 g L⁻¹)

Heavy metal	Isotherm model							
	Langmuir		Freundlich		Temkin		D–R	
	Parameters	ARE	Parameters	ARE	Parameters	ARE	Parameters	ARE
Cu ²⁺	$Q_{max} = 115.48 \text{ mg g}^{-1}$ $K_L = 0.0240 \text{ L mg}^{-1}$	5.11	$K_f = 58.38 \text{ (L mg}^{-1})^{1/n}$ $n = 10.39$	3.78	$K_T = 31.23 \text{ L g}^{-1}$ $Q_{max} = 10.99 \text{ mg g}^{-1}$	4	$Q_{max} = 121.87 \text{ mg g}^{-1}$ $D = 0.001 \text{ mol}^2 \text{ kJ}^{-2}$	5.83
Zn ²⁺	$Q_{max} = 136.33 \text{ mg g}^{-1}$ $K_L = 0.0391 \text{ L mg}^{-1}$	0.3288	$K_f = 112.39 \text{ (L mg}^{-1})^{1/n}$ $n = 42.11$	0.2704	$K_T = 1.04 \times 10^{15} \text{ L g}^{-1}$ $Q_{max} = 3.19 \text{ mg g}^{-1}$	0.2774	$Q_{max} = 135.02 \text{ mg g}^{-1}$ $D = 0.002 \text{ mol}^2 \text{ kJ}^{-2}$	0.40
Pb ²⁺	$Q_{max} = 334.5 \text{ mg/g}$ $K_L = 0.1933 \text{ L mg}^{-1}$	1.18	$K_f = 321.90 \text{ (L mg}^{-1})^{1/n}$ $n = 217.42$	0.7667	$K_T = 9.42 \times 10^{89} \text{ L g}^{-1}$ $Q_{max} = 1.55 \text{ mg g}^{-1}$	0.1408	$Q_{max} = 336.05 \text{ mg g}^{-1}$ $D = 0.0012 \text{ mol}^2 \text{ kJ}^{-2}$	1.54

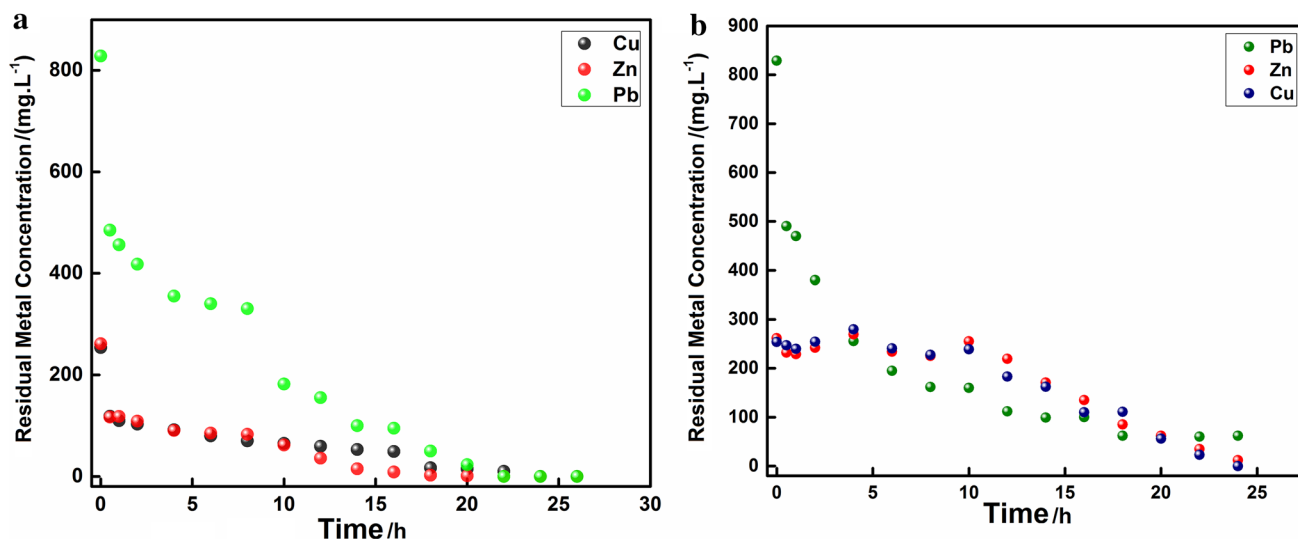


Fig. 8 Variations of residual concentration in **a** single-element and **b** multi-element metal solutions (conditions: initial concentration: 4 mM, adsorbent dose 10 g L⁻¹, Temperature: 25 °C)

Table 6 Constants and ARE of Elovich, second order, and pseudo-second order kinetic models (initial concentration: 4 mM, adsorbent dose 10 g L⁻¹)

Heavy metal	Kinetic model					
	Elovich		Second order		Pseudo-second order	
	Parameters	ARE	Parameters	ARE	Parameters	ARE
Cu ²⁺	$\alpha = 435.76 \text{ mg g}^{-1} \text{ h}^{-1}$ $\beta = 0.3110 \text{ g mg}^{-1}$	3.17	$q_e = 16.92 \text{ mg g}^{-1}$ $k_2 = -0.001 \text{ g mg}^{-1} \text{ h}^{-1}$	10.95	$q_e = 26.09 \text{ mg g}^{-1}$ $k_{2P} = 0.0560 \text{ h}^{-1}$	5.25
Zn ²⁺	$\alpha = 565.70 \text{ mg g}^{-1} \text{ h}^{-1}$ $\beta = 0.3173 \text{ g mg}^{-1}$	4.40	$q_e = 16.86 \text{ mg g}^{-1}$ $k_2 = -0.001 \text{ g mg}^{-1} \text{ h}^{-1}$	8.53	$q_e = 27.34 \text{ mg g}^{-1}$ $k_{2P} = 0.0313 \text{ h}^{-1}$	8.73
Pb ²⁺	$\alpha = 177.02 \text{ mg g}^{-1} \text{ h}^{-1}$ $\beta = 0.066 \text{ g mg}^{-1}$	19.34	$q_e = 42.74 \text{ mg g}^{-1}$ $k_2 = -0.0006 \text{ g mg}^{-1} \text{ h}^{-1}$	10.03	$q_e = 90.62 \text{ mg g}^{-1}$ $k_{2P} = 0.0053 \text{ h}^{-1}$	7.28

It is also possible to evaluate the sorption kinetics from a mechanistic point of view [35, 36]. The overall adsorption process is controlled either by one or more steps (e.g. film diffusion, pore diffusion, etc.) and at a high stirring rate, the diffusive mass transfer with one apparent diffusion coefficient may fit the experimental sorption kinetic data. For an exact surface adsorption, rate variations should be proportional to the first power of concentration; however, when pore diffusion limits adsorption, the relationship between initial solute concentration and the rate of adsorption may become nonlinear [37]. The possibility of intra-particle diffusion can be explored by applying the intra-particle diffusion model (Table 2) to the kinetic data [38]. Values of *I* is attributed to the thickness of the boundary layer and its effect is larger in case of greater intercepts. By applying this model, the data are related by two straight lines (Fig. 9). The deviation of the straight line is the result of the difference in the rate of mass transfer in the initial and final stages of

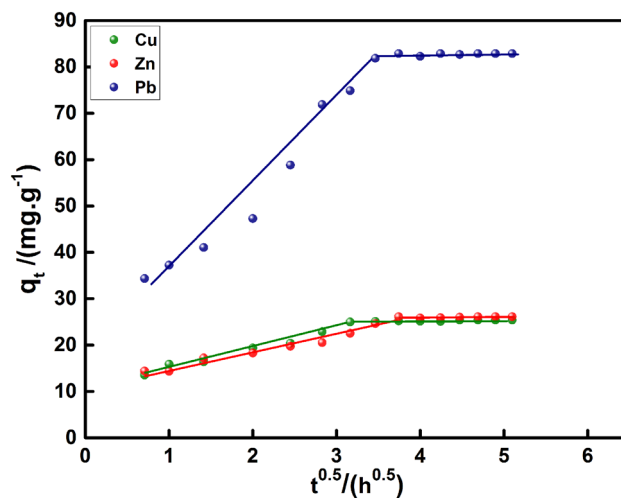


Fig. 9 Weber and Morris intra-particle diffusion plot for sorption of copper, zinc and lead by MTCB (pH₀=5, T=25 °C, adsorbent dose = 10 g L⁻¹, C₀=4 mM)

sorption process; the first line depicts the diffusion in the macropores while the second represents the micropore diffusion. Obviously, Pb^{2+} has larger value of K_{id} (the slope of first line) for diffusion into the porosity which can explain the higher affinity of MTCB for Pb-sorption in comparison with sorption of Cu^{2+} and Zn^{2+} .

The Sorption Mechanisms

Since the pH_{pzc} of MTCB is 6.8, in acidic media, the surface charge of MTCB is positive and this is not in favour of physical adsorption. According to the D–R model and by calculating the mean energy of adsorption (E), Cu^{2+} , Zn^{2+} , and Pb^{2+} sorption result in values that are usually attributed to chemisorption (20.64, 16, and 20.43 Kj mol^{-1} , respectively).

To be more precise, the FT-IR spectra were obtained for metal-loaded MTCB. The post-sorption FT-IR spectrum shows that the wavenumber and intensity of some peaks are shifted to lower values in comparison with the pre-sorption MTCB sample. This suggests that certain functional groups related to the wavenumbers involved play a role in immobilization of metals onto the composite material. In all three loaded samples, the $-\text{NH}_2$ group is involved in the binding of metals, mitigating and shifting the N–H band in MTCB (Fig. 5). Hence, also FT-IR spectra confirm the chemisorption mechanism in case of each metal.

Multi-Element Batch Adsorption Experiments

The simultaneous immobilization of Cu^{2+} , Zn^{2+} , and Pb^{2+} onto MTCB was investigated for the initial concentration of 4 mM for each metal (Fig. 8b). Table 7 represents a comparison for the co-sorption capacity (of Cu, Pb, and Zn) between the base char and MTCB. Obviously, as for equal moles of adsorbents, both base char and MTCB show higher affinity for lead ions. This is also confirmed in the metal distribution pattern obtained in post-sorption specimens using EDS mapping (Fig. 10) where the denser map of Fig. 10c indicates the larger amount of immobilized Pb^{2+} over the MTCB specimen.

Table 7 Comparison of the simultaneous adsorption capacity between the pristine biochar and MTCB (initial metal concentration: 4 mM, adsorbent dose: 10 g L^{-1})

Adsorbent	Sorption capacity (mg g^{-1})		
	Cu^{2+}	Pb^{2+}	Zn^{2+}
Pristine biochar	24.183	63.36	16.38
MTCB nanocomposite	25.42	76.68	24.96

Immobilization of Cu^{2+} , Pb^{2+} , and Zn^{2+} in Soil

A synthetic precipitation leaching procedure was performed for a multi-metal system in a soil amended with 10% w/w MTCB. The results of SPLP test reveal that the proposed novel nanobiocomposite is efficient in immobilizing the metals within the soil environment as it reduces the metal leaching from the soil by 100, 100, and 52.29% for Cu^{2+} , Zn^{2+} , and Pb^{2+} , respectively. This supports the confidence, that this novel material is applicable for use as an efficient soil amendment for mine impacted soils.

Table 8 draws a comparison between the novel MTCB nanobiocomposite and other previously proposed sorbents for Cu^{2+} , Zn^{2+} , and Pb^{2+} immobilization showing the higher loading capacity of MTCB.

Conclusions

In the present study, a novel nanobiocomposite (MTCB) was synthesized and its sorptive behavior towards three specific heavy metals was evaluated both in single and multi-component systems. The main findings are as follows:

- The composite material possesses a mixed organic–inorganic nature: the base biochar has high surface area and its mesoporous structure gives it a unique characteristic as a porous matrix; while the polymer–clay coating imports some active functional groups that are able to efficiently immobilize the heavy metals.
- FT-IR analysis indicates some shifting for active site vibrations of chitosan and montmorillonite nanoclay as a result of exfoliation phenomenon and the interaction of the negatively charged clay surfaces with the active groups of chitosan.
- Single-element experiments show that the sorption isotherm conforms to the Freundlich model in case of Cu^{2+} and Zn^{2+} ; while for Pb^{2+} it is best represented by Temkin model. The mechanism involved in immobilization of heavy metals is determined as binding with active NH_2 groups.
- Moreover, the application of MTCB as a soil amendment was assessed by conducting SPLP tests and the results showed that it can reduce the amount of metal in the leachate through immobilization when added by 10% w/w to the soil.

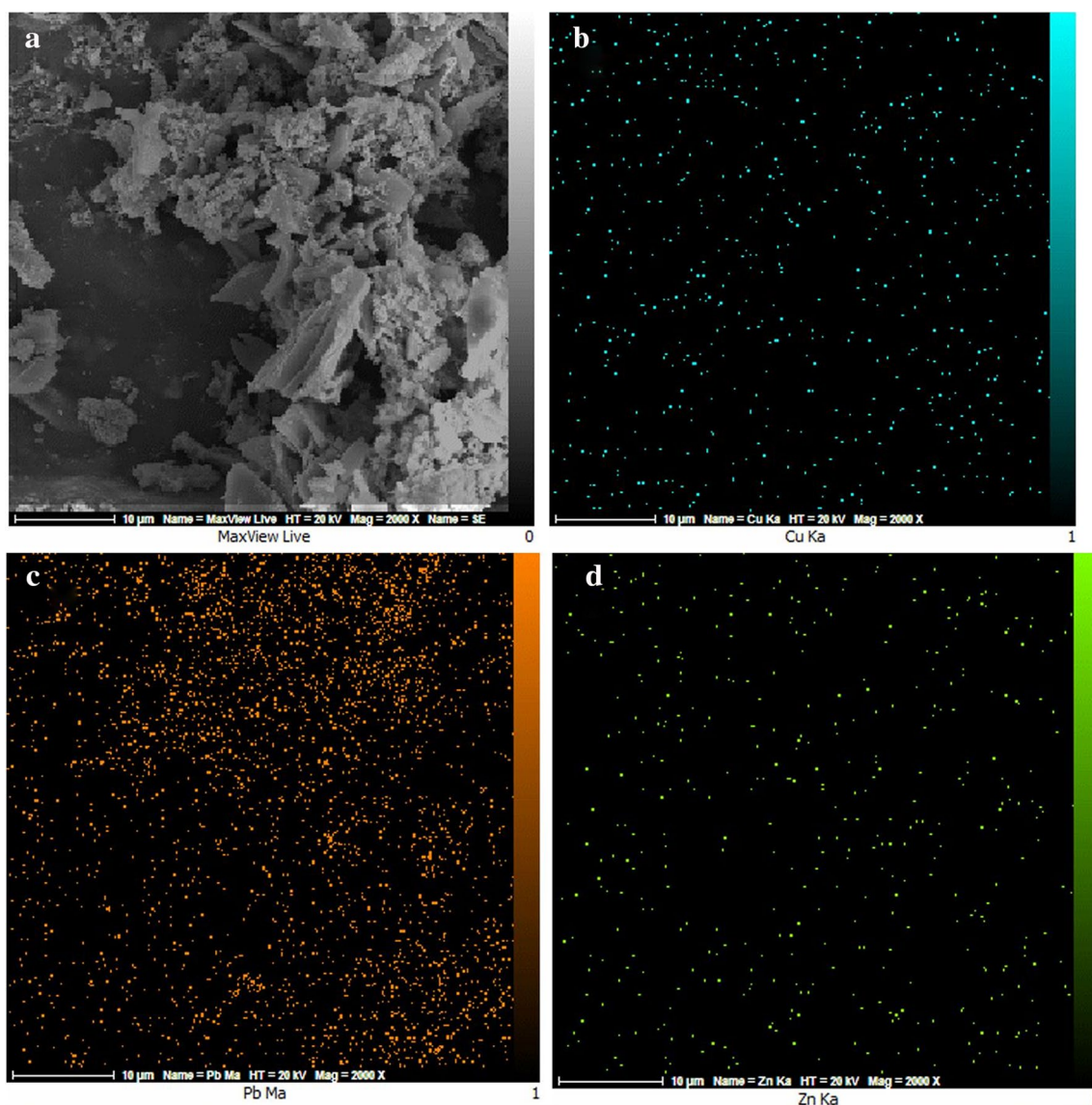


Fig. 10 FE-SEM micrograph showing **a** surface morphology and EDS elemental mapping analysis for **b** Cu^{2+} , **c** Pb^{2+} , and **d** Zn^{2+} distribution over the MTCB specimen

Table 8 Comparison of metal sorption capacity between MTCB and some other sorbents

Adsorbent	Sorption capacity (mg g^{-1})			Ref.
	Cu^{2+}	Pb^{2+}	Zn^{2+}	
MTCB nanocomposite	121.5	336	134.6	Current study
Corn straw biochar	12.52	–	11.0	[34]
Hardwood biochar	6.59	–	4.54	
Chitosan-immobilized on bentonite	12.6	15	–	[39]
Chitosan	59	55.5	–	[40]

Acknowledgements The authors would like to express their sincere thanks to Mazandaran Wood and Paper Industries for their kind cooperation in supply of feedstock materials during this project and also technical helps of Iran Mineral Processing Research Center (IMPRC). The research was financially supported by Iran National Science Foundation (INSF) and Iran Nanotechnology Initiative Council (INIC).

Funding This study was funded by Iran National Science Foundation (INSF) and Iran Nanotechnology Initiative Council (INIC).

Compliance with Ethical Standards

Conflict of interest Hoda Arabyarmohammadi has received research grants from INIC. Ahmad Khodadadi Darban has received research grant from INSF.

Open Access This article is distributed under the terms of the Creative Commons Attribution 4.0 International License (<http://creativecommons.org/licenses/by/4.0/>), which permits unrestricted use, distribution, and reproduction in any medium, provided you give appropriate credit to the original author(s) and the source, provide a link to the Creative Commons license, and indicate if changes were made.

References

- Yang J, Pan X, Zhao C et al (2016) *Geomicrobiol J* 33:261–266
- Georgiev P, Groudev S, Spasova I, Nicolova M (2015) *J Soils Sedim* 16:1288–1299
- Xu R, Zhao A (2013) *Environ Sci Pollut Res Int* 20:8491–8501
- Jeyasingh J, Philip L (2005) *J Hazard Mater* 118:113–120
- Lehmann J, Gaunt J, Rondon M (2006) *Mitig Adapt Strateg Glob Chang* 11:395–419
- Lu H, Zhang W, Yang Y et al (2012) *Water Res* 46:854–862
- Wang H, Gao B, Wang S et al (2015) *Bioresour Technol* 197:356–362
- Wang SF, Shen L, Tong YJ et al (2005) *Polym Degrad Stab* 90:123–131
- Daraei P, Madaeni SS, Salehi E et al (2013) *J Memb Sci* 436:97–108
- Krajewska B (2001) *React Funct Polym* 47:37–47
- Yu-shan XIE, Shao-zao TAN, Ma-hua L, Ren-fu LIU (2010) *Chem Res Chin Univ* 26:509–513
- Vanamudan A, Pamidimukkala P (2015) *Int J Biol Macromol* 74:127–135
- Auta M, Hameed BH (2014) *Chem Eng J* 237:352–361
- Monvisade P, Siriphannon P (2009) *Appl Clay Sci* 42:427–431
- Kittinaovarat S, Kansomwan P, Jiratumnukul N (2010) *Appl Clay Sci* 48:87–91
- Hussein OT (2015) *Int J Sci Eng Appl* 4:174–185
- Pandey S, Mishra SB (2011) *J Colloid Interface Sci* 361:509–520
- Sabaa MW, Abdallah HM, Mohamed N a., Mohamed RR (2015) *Mater Sci Eng C* 56:363–373
- Bleiman N, Mishael YG (2010) *J Hazard Mater* 183:590–595
- Kuo S (1996) Phosphorus. In: Sparks DL, Page AL, Helmke PA eds. *Methods soil anal. Part 3—chemical methods*, RHL, Madison, pp 869–919
- Balistreri LS, Murray JW (1981) *Am J Sci* 281:788–806
- Srivastava VC, Mall ID, Mishra IM (2008) *Chem Eng Process Process Intensif* 47:1269–1280
- Arabyarmohammadi H, Salarirad MM, Behnamfard A (2014) *Environ Prog Sustain Energy* 33:777–789
- Temkin MJ, Pyzhev TV (1940) *Acta Physiochim USSR* 12:217–222
- Sousa Neto VO, Oliveira AG, Teixeira RNP et al (2011) *BioResources* 6:3376–3395
- Mayer ZA, Eltom Y, Stennett D et al (2014) *Environ Prog Sustain Energy* 33:490–496
- Enders A, Hanley K, Whitman T et al (2012) *Bioresour Technol* 114:644–653
- Bansal RC, Goyal M (2005) *Activated carbon adsorption*, CRC press, Boca Raton
- Sing KSW (1985) *Pure Appl Chem* 57:603–619
- Sirousazar M, Kokabi M, Hassan ZM, Bahramian AR (2011) *Sci Iran* 18:780–784
- Xu Y, Ren X, Hanna MA (2006) *J Appl Polym Sci* 99:1684–1691
- Choi Y, Shin SYA, Soares JBP (2010) *Macromol Chem Phys* 211:1026–1034
- Liu Z, Zhang F-S (2009) *J Hazard Mater* 167:933–939
- Chen X, Chen G, Chen L et al (2011) *Bioresour Technol* 102:8877–8884
- Plazinski W, Dziuba J, Rudzinski W (2013) *Adsorption* 19:1055–1064
- Ho YS, McKay G (1998) *Process Saf Environ Prot* 76:332–340
- Singh TS, Pant K (2004) *Sep Purif Technol* 36:139–147
- Mall ID, Srivastava VC, Kumar GV a, Mishra IM (2006) *Colloids Surf A Physicochem Eng Asp* 278:175–187
- Futalan CM, Tsai W, Lin S, Hsien K (2012) *Sustai Environ Res* 22(6):345–355
- Sobhanardakani S, Zandipak R, Parvizimosaed H, Khoei AJ, Moslemi M, Tahergorabi M, Hosseini SM, Delfieh P (2014) *Iran J Toxicol* 8(26):1145–1151